

# Diffusion-Weighted MRI in the Body: Applications and Challenges in Oncology

Dow-Mu Koh<sup>1,2</sup>  
David J. Collins<sup>1,2</sup>

**OBJECTIVE.** In this article, we present the basic principles of diffusion-weighted imaging (DWI) that can aid radiologists in the qualitative and quantitative interpretation of DW images. However, a detailed discussion of the physics of DWI is beyond the scope of this article. A short discussion ensues on the technical aspects of performing DWI in the body. The emerging applications of DWI for tumor detection, tumor characterization, distinguishing tumor tissue from nontumor tissue, and monitoring and predicting treatment response are highlighted. The challenges to widespread adoption of the technique for cancer imaging in the body are discussed.

**CONCLUSION.** DWI derives its image contrast from differences in the motion of water molecules between tissues. Such imaging can be performed quickly without the need for the administration of exogenous contrast medium. The technique yields qualitative and quantitative information that reflects changes at a cellular level and provides unique insights about tumor cellularity and the integrity of cell membranes. Recent advances enable the technique to be widely applied for tumor evaluation in the abdomen and pelvis and have led to the development of whole-body DWI.

**F**or two decades, diffusion-weighted imaging (DWI) has been applied to the evaluation of intracranial diseases, such as cerebrovascular accidents, trauma, epilepsy, depression, dementia, and neurotoxicity. DWI has been shown to be capable of detecting early or subtle changes within the brain before any visible abnormality can be seen on conventional morphologic imaging [1, 2].

In the 1990s, a series of technologic advances made it possible to translate DWI measurements to extracranial sites, including the abdomen and pelvis. The developments of echo-planar imaging (EPI), high-gradient amplitudes, multichannel coils, and parallel imaging have been instrumental in extending the applications of DWI. In particular, the introduction of parallel imaging, which enabled reduction in the TE, the echo-train length, and the k-space filling time, led to substantially less motion artifact at image acquisition, thus enabling high-quality DW images of the body to be obtained.

DWI is increasingly used for the evaluation of extracranial diseases. There is growing interest in the application of DWI for the evaluation of the patient with cancer. DWI measurements are quick to perform (typically 1–5

minutes) and do not require the administration of exogenous contrast medium. Thus, these imaging sequences can be appended to existing imaging protocols without a significant increase in the examination time. Furthermore, DWI yields both qualitative and quantitative information that can be helpful for tumor assessment.

## Principles and Concepts

In the following section, we summarize the key concepts of DWI, which may aid radiologists in the interpretation of DW images. However, an in-depth discussion of the physics and mathematics of DWI is beyond the scope of this review. The interested reader may refer to articles related to that subject [3, 4].

### *Diffusion of Water Molecules in Tissue*

DWI explores the random motion of water molecules in the body. Water molecules held in a container outside the body are in constant random brownian motion. This uninhibited motion of water molecules is free diffusion. By contrast, the movement of water molecules in biologic tissues is restricted because their motion is modified and limited by interactions with cell membranes and macromolecules.

**Keywords:** abdominal imaging, cancer, diffusion-weighted imaging, MRI, oncologic imaging, pelvic imaging, whole-body imaging

DOI:10.2214/AJR.06.1403

Received October 22, 2006; accepted after revision January 26, 2007.

Supported by Cancer Research UK Grant C1060/A5117.

<sup>1</sup>Cancer Research UK Clinical Magnetic Resonance Research Group, Institute of Cancer Research, Sutton, Surrey, United Kingdom.

<sup>2</sup>Academic Department of Radiology, Royal Marsden Hospital, Downs Rd., Sutton, Surrey SM2 5PT, United Kingdom. Address correspondence to D. M. Koh.

*AJR* 2007; 188:1622–1635

0361–803X/07/1886–1622

© American Roentgen Ray Society

## DWI Applications and Challenges in Oncology

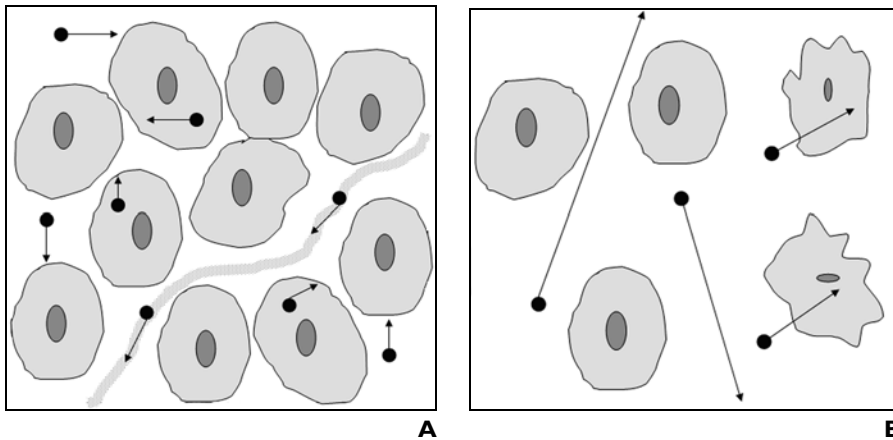


**Fig. 1**—Diffusion of water molecules.

**A**, Restricted diffusion: cellularity and intact cell membranes. Drawing represents 1 voxel of tissue evaluated by diffusion-weighted imaging (DWI) containing cells and blood vessel. Note water molecules (black circles with arrows) within extracellular space, intracellular space, and intravascular space, all of which contribute to measured MR signal. In this highly cellular environment, water diffusion is restricted because of reduced extracellular space and by cell membranes, which act as barrier to water movement.

**B**, Free diffusion: low cellularity and defective cell membranes. In less cellular environment, relative increase in extracellular space allows freer water diffusion than more cellular environment would. Defective cell membranes also allow movement of water molecules between extracellular and intracellular spaces.

The degree of restriction to water diffusion in biologic tissue is inversely correlated to the tissue cellularity and the integrity of cell membranes [6–9]. The motion of water molecules is more restricted in tissues with a high cellular density associated with numerous intact cell membranes (e.g., tumor tissue). The lipophilic cell membranes act as barriers to motion of water molecules in both the extracellular and intracellular spaces. By contrast, in areas of low cellularity or where the cellular membrane has been breached, the motion of water molecules is less restricted. A less cellular environment provides a larger extracellular space for diffusion of water molecules, and these molecules may also freely transgress defective cell membranes to move from the extracellular into the intracellular compartment (Fig. 1).

### Measuring Water Motion (Apparent Diffusion) Using DWI

Stejskal and Tanner [10] described an MR experiment that could be applied to the detection and quantification of water diffusion in vivo. They adapted a standard T2-weighted spin-echo sequence by applying a symmetric pair of diffusion-sensitizing (bipolar) gradients around the 180° refocusing pulse. That approach is now the basis of many DWI sequences in clinical use today. Static molecules acquire phase information from the first diffusion gradient, but information will be rephased by the second diffusion gradient without a significant change in the measured signal intensity. By comparison, moving water molecules acquire different phase information from the first gradient, but because of their motion, their signal will not be completely rephased by the second gradient, thus leading to a signal loss (Fig. 2). Hence, the motion of water molecules is detected as attenuation of the measured signal intensity at DWI. The degree of water motion has been found to be proportional to the degree of signal attenuation.

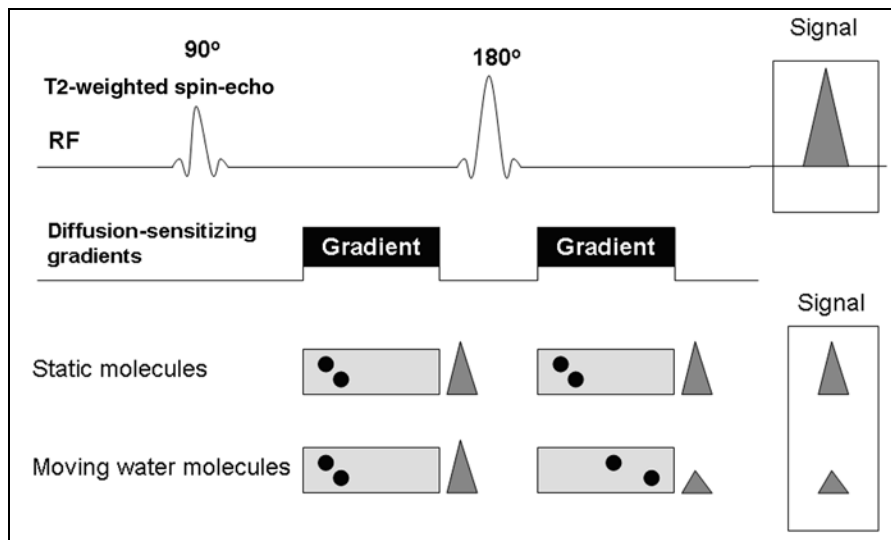


**Fig. 2**—Measuring water diffusion. Stejskal and Tanner [10] adopted T2-weighted spin-echo sequence for measuring water diffusion. They applied symmetric diffusion-sensitizing gradient around 180° refocusing pulse. On this schematic drawing, stationary molecules are unaffected by gradients and measured signal intensity is preserved. By contrast, moving water molecules acquire phase information from first gradient, which is not entirely rephased by second gradient, thereby leading to signal loss. Hence, water diffusion is detected as attenuation of measured MR signal intensity. RF = radiofrequency pulse.

In biologic tissue, the DWI signal is derived from the motion of water molecules in the extracellular space, the intracellular space, and the intravascular space [4] (Fig. 1). Not surprisingly, given a unit time, water molecules in the intravascular space will have a greater diffusion distance because of blood flow than

those in the extracellular and intracellular spaces. Clearly, the contribution of intravascular water diffusion to the measured DWI signal can vary among tissues. In tumors showing increased vascularity, the contribution of intravascular water diffusion to the MR signal may account for a significant proportion [5].

The sensitivity of the DWI sequence to water motion can be varied by changing the gradient amplitude, the duration of the applied gradient, and the time interval between the paired gradients. On clinical MR scanners, the diffusion sensitivity is easily varied by changing the parameter known as the “b value,” which is proportional to these three factors. When the b value is changed, it is usually the gradient amplitude, rather than the duration or time intervals between gradients, that is altered.

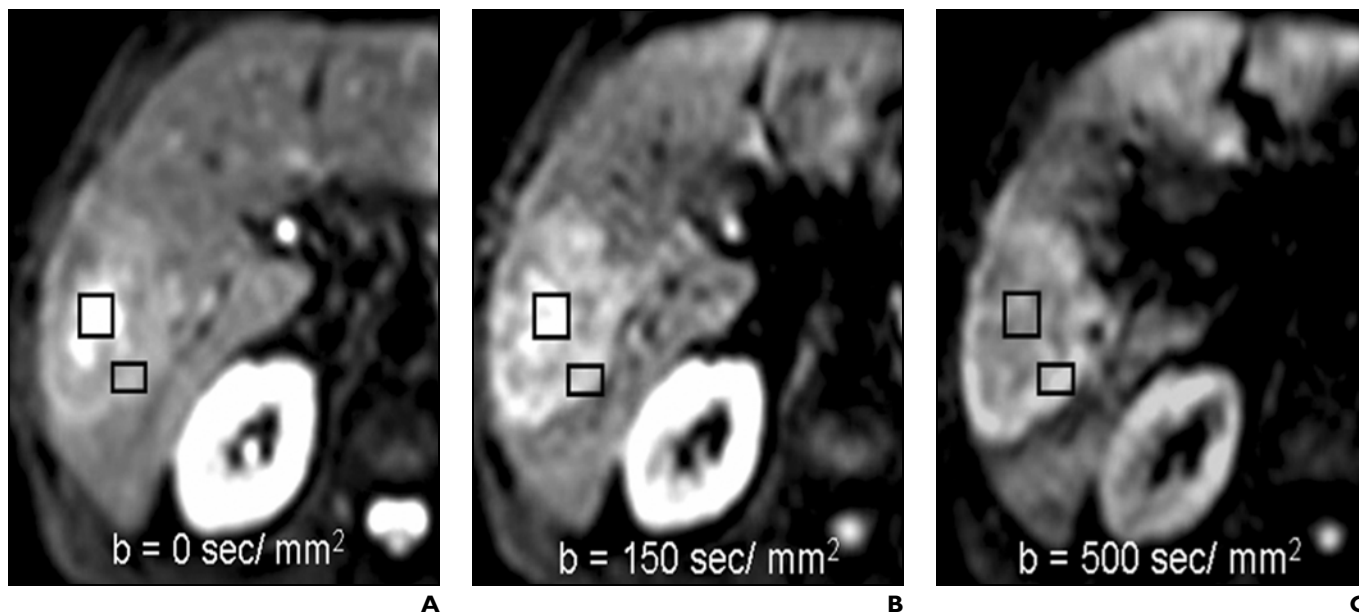


**Fig. 3**—Tissue characterization by diffusion-weighted images.

**A–C**, Diffusion-weighted MR images in 55-year-old man with liver metastasis obtained at different  $b$  values show large heterogeneous metastasis within right lobe of liver. Necrotic center of metastasis (*squares*) shows attenuation of signal intensity with increasing  $b$  values, indicating less restricted diffusion. By comparison, rim of tumor (*rectangles*) is more cellular and shows little signal attenuation with increasing  $b$  value.

Water molecules with a large degree of motion or a great diffusion distance (e.g., within the intravascular space) will show signal attenuation with small  $b$  values (e.g.,  $b = 50\text{--}100\text{ s/mm}^2$ ). By contrast, large  $b$  values (e.g.,  $b = 1,000\text{ s/mm}^2$ ) are usually required to perceive slow-moving water molecules or small diffusion distances because these show more gradual signal attenuation with increasing  $b$  values.

The root mean square displacement of water molecules that occurs during a diffusion measurement is estimated to be approximately  $8\text{ }\mu\text{m}$  [11]. By comparison, the mean size of cells in the human body measures about  $10\text{ }\mu\text{m}$ . Hence, the information provided by DWI reflects changes that are occurring at a cellular spatial scale. For this reason, DWI is perceived as an advantageous tool for evaluating changes in the tumor microenvironment, both before and after treatment.

### Interpretation of DWI

#### Qualitative Assessment of DWI

DWI is typically performed using at least two  $b$  values (e.g.,  $b = 0\text{ s/mm}^2$  and other  $b$  values from 0 to  $1,000\text{ s/mm}^2$ ) to enable meaningful interpretation. Generally, the larger the  $b$  value, the greater the degree of signal attenuation from water molecules. By observing the relative attenuation of signal intensity

on images obtained at different  $b$  values, tissue characterization based on differences in water diffusion becomes possible. For example, in a heterogeneous tumor, the more cystic or necrotic fraction of the tumor will show greater signal attenuation on high  $b$ -value images because water diffusion is less restricted. By contrast, the more cellular solid tumor areas will continue to show relatively high signal intensity (Fig. 3). Visual assessment of the relative tissue signal attenuation at DWI is being applied for tumor detection, tumor characterization, and the evaluation of treatment response in patients with cancer.

When diffusion measurements are being performed, the direction of water diffusion along the three orthogonal directions of the magnet (phase select, frequency select, and slice select) can be assessed independently by applying diffusion gradients in each of these directions. DW images that are the sum of the directionally acquired DW images are known as trace or index DW images.

One of the pitfalls of visual assessment of directional or index DW images is that the signal intensity observed depends on both water diffusion and the T2 relaxation time. Consequently, an area with a very long T2 relaxation time may remain high signal at DWI and be mistaken for restricted diffusion. This is known as the “T2 shine-

through” effect (Fig. 4). This effect can be sometimes reduced by the choice of an appropriate TE (a short one) and  $b$  value (a large one), but it cannot be easily avoided. The relative contribution of T2 signal intensity to DW images is a potential source of error in image interpretation and can limit their usefulness when comparing results among studies performed using different imaging protocols. A simple solution to the problem of T2 shine-through can be found using the exponential image. The exponential image is formed by taking the ratio of a DW image divided by an unweighted image ( $b = 0\text{ s/mm}^2$ ) from the same image series and slice position.

Another phenomenon that can be encountered is that of diffusion anisotropy. Diffusion anisotropy refers to unequal directional diffusion, which occurs as a result of tissue or structural organization. A good example of diffusion anisotropy is seen along the white matter tracts of the internal capsule in the brain. The diffusion motion appears relatively free in the head-foot direction along the long axis of the white matter tracts, but appears restricted in the anteroposterior and right-left directions across the neuronal fibers. In the assessment of tumors, diffusion anisotropy can help to identify tumor invasion of adjacent structures [12]. However,

## DWI Applications and Challenges in Oncology

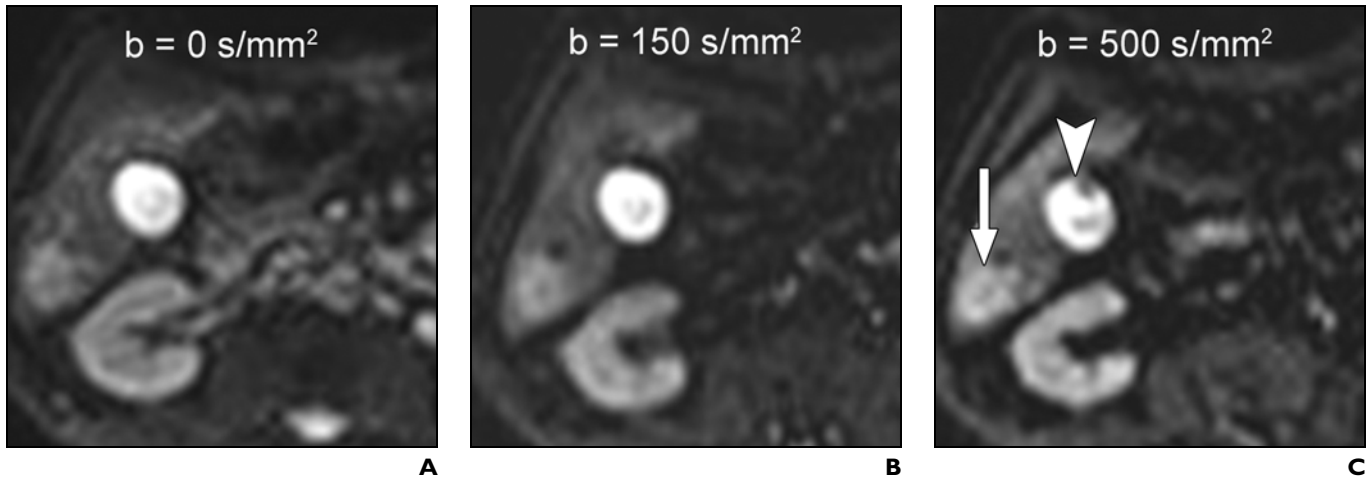


**Fig. 4**—T2 shine-through.

**A–C**, Diffusion-weighted images of liver in 62-year-old man with liver metastasis obtained at different  $b$  values show ill-defined high-signal-intensity metastasis in right lobe of liver (arrow, **C**). However, note gallbladder (arrowhead, **C**) also shows high signal intensity, even on image obtained with  $b$  value of 500  $\text{s/mm}^2$ . In this case, high signal intensity of gallbladder is not due to restricted water diffusion but to T2 shine-through. Note intrinsic high signal intensity of gallbladder on T2-weighted ( $b = 0 \text{ s/mm}^2$ ) image (**A**) due to its long T2 relaxation time.

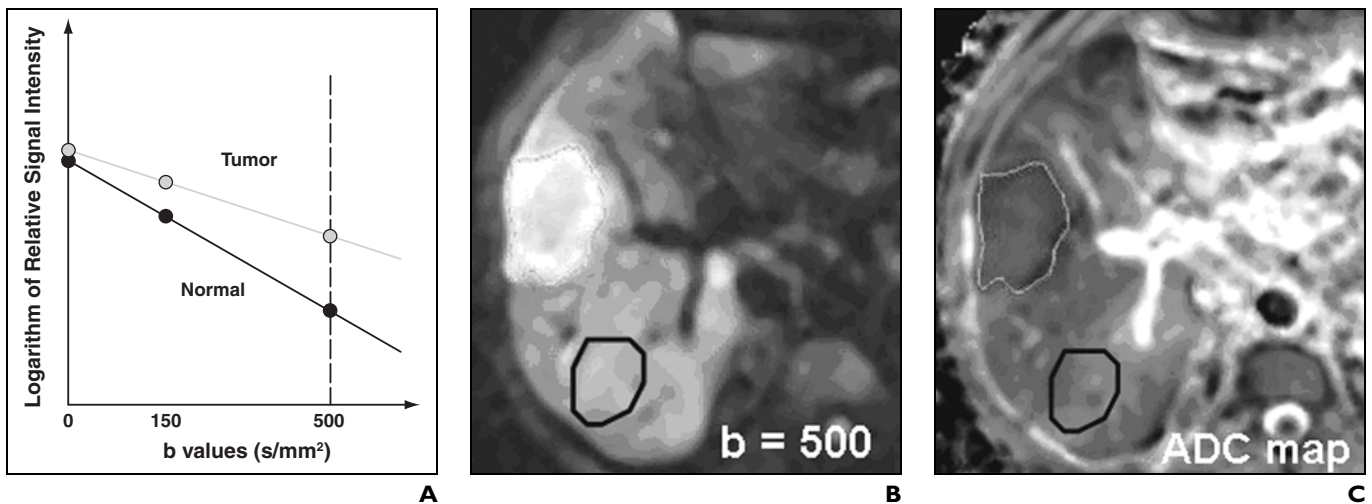


**Fig. 5**—Apparent diffusion coefficient (ADC).

**A**, Simplified schematic shows derivation of ADC. Logarithm of relative signal intensity is plotted on  $y$ -axis against values on  $x$ -axis. Slope of line fitted through plots is ADC. In this example, slope of line (ADC) is smaller for tumor (gray line) than for normal liver (black line).

**B** and **C**, Tumor area with low ADC (gray outline) is darker than normal liver with higher ADC (black outline). Note contrast on ADC map is opposite that seen on diffusion-weighted image. On diffusion-weighted image, tumor showed less signal attenuation and appeared higher signal intensity than normal liver. **B** and **C** obtained in 45-year-old man with liver metastasis.

diffusion in tumors is usually isotropic because malignant cells typically grow in a disorganized fashion.

### Quantitative Analysis of DWI

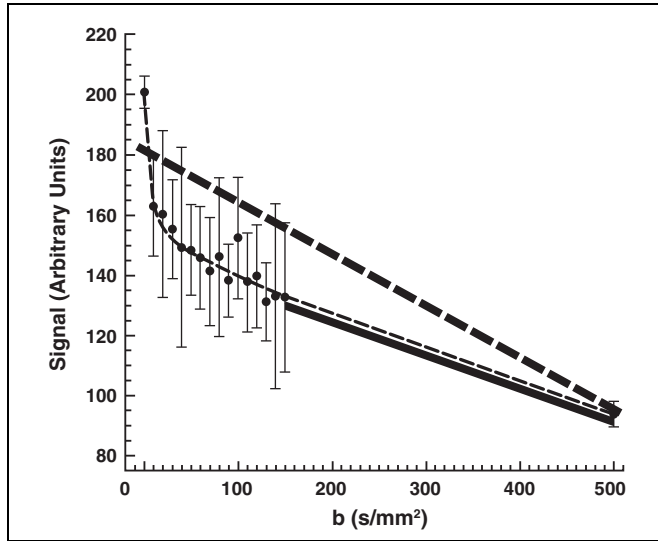
By performing DWI using different  $b$  values, quantitative analysis is possible. This analysis is usually performed at a push of a button on the scanner or workstation that results in the calculation of the apparent diffusion coefficient (ADC) (Appendix 1). One

simplified method of visualizing this process is by considering the signal attenuation of a tissue with increasing  $b$  values. By plotting the logarithm of the relative signal intensity of the tissue on the  $y$ -axis against the  $b$  values on the  $x$ -axis, a line can be fitted through the plots (exponential function). The slope of the line describes the ADC (Fig. 5). Not surprisingly, the fit can be improved by using more  $b$  values to reduce the error in ADC calculation.

The ADC is independent of magnetic field strength and can overcome the effects of T2 shine-through, thus allowing more meaningful comparison of results. The ADC is calculated for each pixel of the image and is displayed as a parametric map. By drawing regions of interests on these maps, the ADCs of different tissues can be derived.

Areas of restricted diffusion in highly cellular areas show low ADC values compared with less cellular areas that return higher

**Fig. 6**—Diffusion-weighted imaging in liver. Graph shows signal attenuation of normal liver with increasing b values (*thin dashed line*). Note there is initial rapid attenuation of signal intensity with small increase in b value from zero. This is due to nulling of signal contribution from capillary perfusion. Slope of line (*thick dashed line*) fitted through all b values describes apparent diffusion coefficient (ADC). However, slope of line (*thick solid line*) fitted through only higher b values (e.g., 150–500 mm<sup>2</sup>/s) can be used to describe perfusion-insensitive ADC. Error bars show 95% CI of pixel values.



ADC values. At this point, it is important to mention that although areas of restricted diffusion will appear to be higher in signal intensity on the directional or index DW images, these areas will appear as low-signal-intensity areas (opposite to DW images) on the ADC map (Fig. 5).

However, it is simplistic to assume that the attenuation of the signal intensity with increasing b values occurs linearly in tissues. In the liver, the signal intensity can be seen initially to attenuate rapidly with low b values, followed by a more gradual signal reduction (Fig. 6). The initial reduction in signal intensity is believed to be due to vascular capillary perfusion, where the signal from fast-moving water molecules is rapidly attenuated by low diffusion weighting [4]. Thus, diffusion-weighted data acquired over a range of b values that includes low b values (< 50 s/mm<sup>2</sup>) are sensitive to signal attenuation from perfusion.

From the previous discussion, it stands to reason that deriving a flow-sensitive ADC value and a flow-insensitive ADC value is possible [4]. An exponential function fitted across all the b values describes the conventional ADC (flow sensitive). However, an exponential function fitted through only the high b values (e.g., b = 150–500 s/mm<sup>2</sup>) can be used to describe a flow-insensitive ADC. The flow-insensitive ADC may potentially provide a more accurate estimate of the cellularity of the tumor microenvironment by minimizing any vascular contributions (Fig. 6). As a further refinement, a biexponential function may be used to calculate conventional ADC from DWI that includes low b values [4].

In the brain, the presence of highly organized anatomic structures allows a particular quantitative diffusion technique, diffusion tensor imaging, to be used to advantage. Diffusion tensor imaging yields information about both the rate and the direction of water diffusion by sampling water motion in at least six directions. The potential application of diffusion tensor imaging in organs with discernible structural organization, such as the prostate and kidneys, is currently being evaluated [13–15].

**Clinical DWI in the Body: Technical Issues**

A range of imaging sequences and techniques are now available for performing DWI studies in the body. The principles of these imaging sequences will not be discussed in this re-

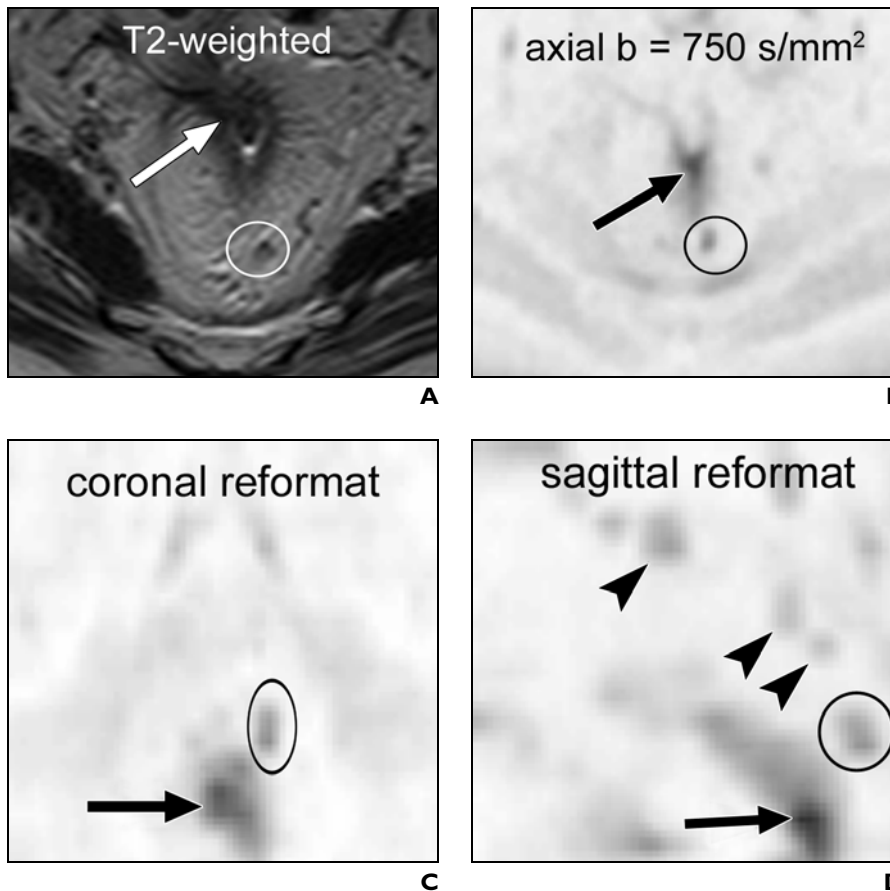


**Fig. 7**—Diffusion-weighted imaging (DWI) performed during free-breathing of 65-year-old man with rectal cancer. **A–D**, Thin-partition DWI can be achieved using free-breathing technique. In this example, axial image with b value of 750 s/mm<sup>2</sup> (**B**) is displayed using inverted gray scale; image shows areas of restricted diffusion corresponding to area of rectal tumor (*arrows*) and 4-mm mesorectal lymph node (*circles*). Thinner slice partition allows multiplanar reformats for anatomic localization. Addition perirectal nodes (*arrowheads*, **D**) are also visible on sagittal reformatted image (**D**). Note corresponding features on T2-weighted MRI (**A**).

## DWI Applications and Challenges in Oncology

**TABLE 1: Diffusion-Weighted Imaging (DWI) Sequences for Evaluating Tumors in the Abdomen and Pelvis<sup>a</sup>**

Parameter	Applications		
	Imaging of the Liver, Abdomen, and Pelvis		Whole-Body Imaging Using Non-Breath-Hold DWI
	Breath-Hold DWI	Non-Breath-Hold DWI	
Field of view (cm)	340–400	340–400	380–400
Matrix size	112 × 256	112 × 256	160 × 256
TR (ms)	> 2,000	3,900	> 3,500
TE (ms)	56–68	78	72
Fat suppression	SPAIR	SPAIR or STIR	STIR
Echo-planar imaging factor	65	59	47
Parallel imaging factor	2	2	2
No. of signals averaged	Single-shot	5	6
Section thickness (mm)	7 <sup>b</sup>	5	4 <sup>c</sup>
Directions of motion probing gradients	Phase, frequency, and slice	Phase, frequency, and slice	Phase, frequency, and slice
b factors (s/mm <sup>2</sup> )	0, 150, and 500	0, 50, 100, 250, 500, and 750	0 and 1,000
Others remarks	May be performed as non-breath-hold respiratory- or navigator-triggered sequence; is especially useful for imaging the liver	Versatile for qualitative and quantitative analyses	Can also be applied to imaging of the abdomen and pelvis; may be less useful for ADC quantification

Note—SPAIR = spectral inversion recovery.

<sup>a</sup>Imaging protocols as implemented on a 1.5-T MR system.

<sup>b</sup>Contiguous.

<sup>c</sup>With 1-mm overlap.

view, and the reader may want to refer elsewhere [16]. The range of imaging techniques includes conventional spin-echo and stimulated echo, fast spin-echo, gradient-echo (e.g., steady-state free precession), EPI, and line scan diffusion imaging [16]. Each of these techniques has its advantages and limitations [16].

In the implementation of DWI in the body, two main strategies can be pursued: breath-hold imaging and non-breath-hold imaging. Breath-hold imaging allows a target volume (e.g., liver, kidney, and elsewhere in the abdomen) to be rapidly assessed. The images retain good anatomic detail and are usually not degraded by respiratory motion or volume averaging. Small lesions may be better perceived and the quantification of ADC is theoretically more accurate than with a non-breath-hold technique. One example of such a technique is breath-hold single-shot spin-echo EPI combined with parallel imaging (e.g., sensitivity encoding) and fat suppression [17–22]. The image acquisition time at each breath-hold is 20–30 seconds, and imaging is typically completed in a few breath-holds. The disadvantages of breath-hold imaging include a limited number of b-value images that can be acquired over the duration of a breath-hold, poorer signal-to-noise ratio compared with multiple averaging methods, and greater sensitivity to pulsatile and susceptibility artifacts.

Non-breath-hold spin-echo EPI combined with fat suppression is a versatile technique that can be used as a general purpose DWI sequence in the body and for whole-body imaging [23]. Multiple slice excitation and signal averaging over a longer duration improve the signal-to-noise and contrast-to-noise ratios [23]. Thin partitions can be achieved (4–5 mm), thus improving spatial resolution and enabling multiplanar image reformats (Fig. 7). Furthermore, the longer acquisition time with non-breath-hold imaging provides flexibility in the use of multiple (> 5) or of high b values; for example, a b value of 1,000 s/mm<sup>2</sup> is optimum for optimum background suppression in whole-body imaging. However, the image acquisition time using this technique is longer compared with breath-hold imaging, typically 3–6 minutes depending on the coverage required and the number of b values used, and evaluation of tumor heterogeneity may be compromised by the degree of motion and volume averaging. Table 1 provides illustrative examples of breath-hold and non-breath-hold imaging sequences that may be applied for tumor evaluation in the body.

Despite the numerous advances in hardware and software, meticulous technique is still needed to minimize bulk motion artifacts that can significantly degrade image quality. When performing DWI in the body, the acqui-

sition time should be kept as short as possible. Depending on the tissue being investigated, the TR should be long enough to minimize T1 saturation effects. However, it should be borne in mind that DWI sequences applied to imaging in the body may have inherent trade-offs because of the need for short acquisition times, and radiologists should be acquainted with these when prescribing their use and when interpreting images.

### Applications of DWI in the Body for Tumor Assessment

DWI yields qualitative and quantitative information that provides unique insight into tumor characteristics, and there is growing evidence for its use in the assessment of the patient with cancer.

#### Tumor Detection

Tumors are frequently more cellular than the tissue from which they originate and thus appear to be of relatively high signal intensity (restricted diffusion) at DWI.

DWI is being applied for the detection of liver metastases. In the liver, low b-value images (e.g., b = 50–150 s/mm<sup>2</sup>) that suppress the high-signal flow from the hepatic vessels, resulting in black blood images, have been found to be useful for lesion detection [24] (Fig. 8). Metastases appear as high-signal-intensity foci at DWI.

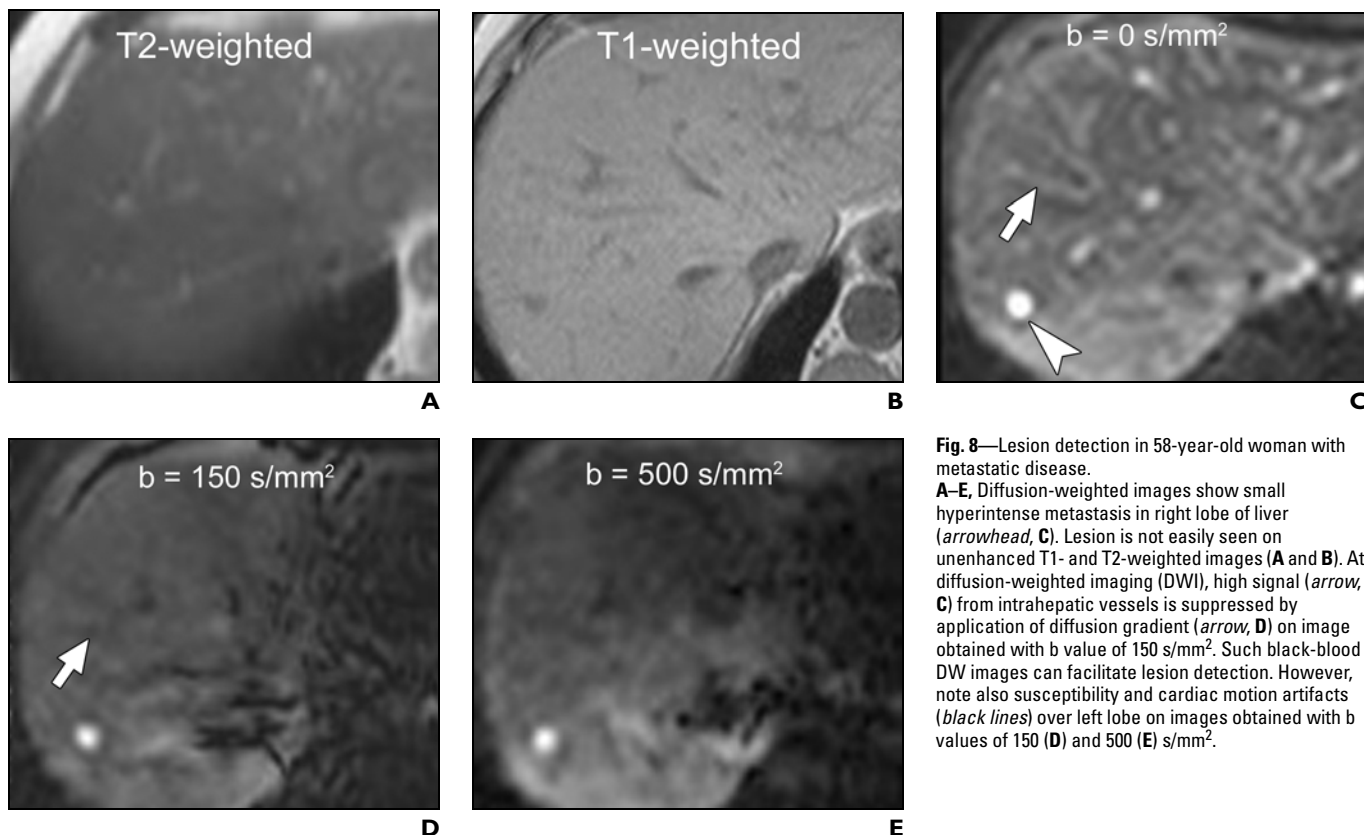


**Fig. 8**—Lesion detection in 58-year-old woman with metastatic disease. **A–E**, Diffusion-weighted images show small hyperintense metastasis in right lobe of liver (*arrowhead, C*). Lesion is not easily seen on unenhanced T1- and T2-weighted images (**A** and **B**). At diffusion-weighted imaging (DWI), high signal (*arrow, C*) from intrahepatic vessels is suppressed by application of diffusion gradient (*arrow, D*) on image obtained with b value of 150 s/mm<sup>2</sup>. Such black-blood DW images can facilitate lesion detection. However, note also susceptibility and cardiac motion artifacts (*black lines*) over left lobe on images obtained with b values of 150 (**D**) and 500 (**E**) s/mm<sup>2</sup>.

Nasu et al. [25] found that DWI was more accurate than superparamagnetic iron oxide (SPIO)-enhanced MRI for the detection of liver metastases. In that study, the sensitivity and specificity of SPIO-enhanced MRI were 66% and 90%, respectively. By comparison, DWI was found to have a higher sensitivity of 82% and specificity of 94%. In another study, DWI was found to have a similarly high sensitivity of 86% and specificity of 94% for the detection of colorectal hepatic metastases [26].

Some of the challenges encountered in DWI of the liver are cardiac motion and susceptibility artifacts that can obscure or diminish visualization of the left lobe (Fig. 7). The susceptibility effects may result from air in the adjacent stomach or colon. Artifacts resulting from cardiac motion can be reduced by triggered acquisition by ECG or a peripheral pulse unit, thus improving image quality and signal-to-noise ratio in the left lobe of the liver [27, 28]. Images may also be acquired with the aid of respiratory triggering to minimize inadvertent breathing motion. However, these techniques increase the image acquisition time, which can render the examination more susceptible to bulk motion.

#### Tumor Characterization

Tumors differ in their cellularity, and this difference may reflect their histologic composition and biologic aggressiveness. The use of DWI for tumor characterization was first shown in brain tumors. The interested reader might like to refer to a more in-depth account of the use of DWI in the evaluation of intracranial tumors [29], which is beyond the scope of this article.

To characterize lesions in the liver using DWI, b values ranging between 0 and 500 s/mm<sup>2</sup> are appropriate [25, 30]. Qualitative visual assessment can help to distinguish cystic from solid lesions (Fig. 9). However, it is often difficult to distinguish different types of solid lesions from one another in the liver by visual assessment alone. For example, a hemangioma will exhibit restricted diffusion and can mimic the appearance of a metastasis at DWI (Fig. 9).

Using quantitative evaluation, investigators have found that benign liver lesions, such as cysts and hemangiomas, have higher mean ADC values (e.g.,  $2.45 \times 10^{-3}$  mm<sup>2</sup>/s) than malignant lesions, such as metastases and hepatocellular carcinoma (e.g.,  $1.08 \times 10^{-3}$

mm<sup>2</sup>/s) [31, 32]. The ADC has also been used to distinguish abscesses, which have low ADC values, from cystic and necrotic metastases, which have higher ADC values [33]. However, although the ADC values differ in summary statistics between benign and malignant lesions, using an individual ADC value to characterize lesions prospectively can be difficult. This difficulty is due to the considerable overlap in the ADC values of benign and malignant abnormalities. The wide range of ADCs in tumors may be explained by biologic variations of tumors, which become even more obvious across studies. For example, although some researchers have reported that metastases have lower ADC values than liver [31], others have found the ADCs of metastases to be higher than that of liver [34, 35]. Another possible reason for the wide range of ADC values may be errors in the measurements and image analysis. Hence, for the time being, DWI of the liver for lesion characterization should be combined with all available imaging to make the optimal assessment.

In the abdomen, DWI has also been applied to characterize focal renal lesions [18,

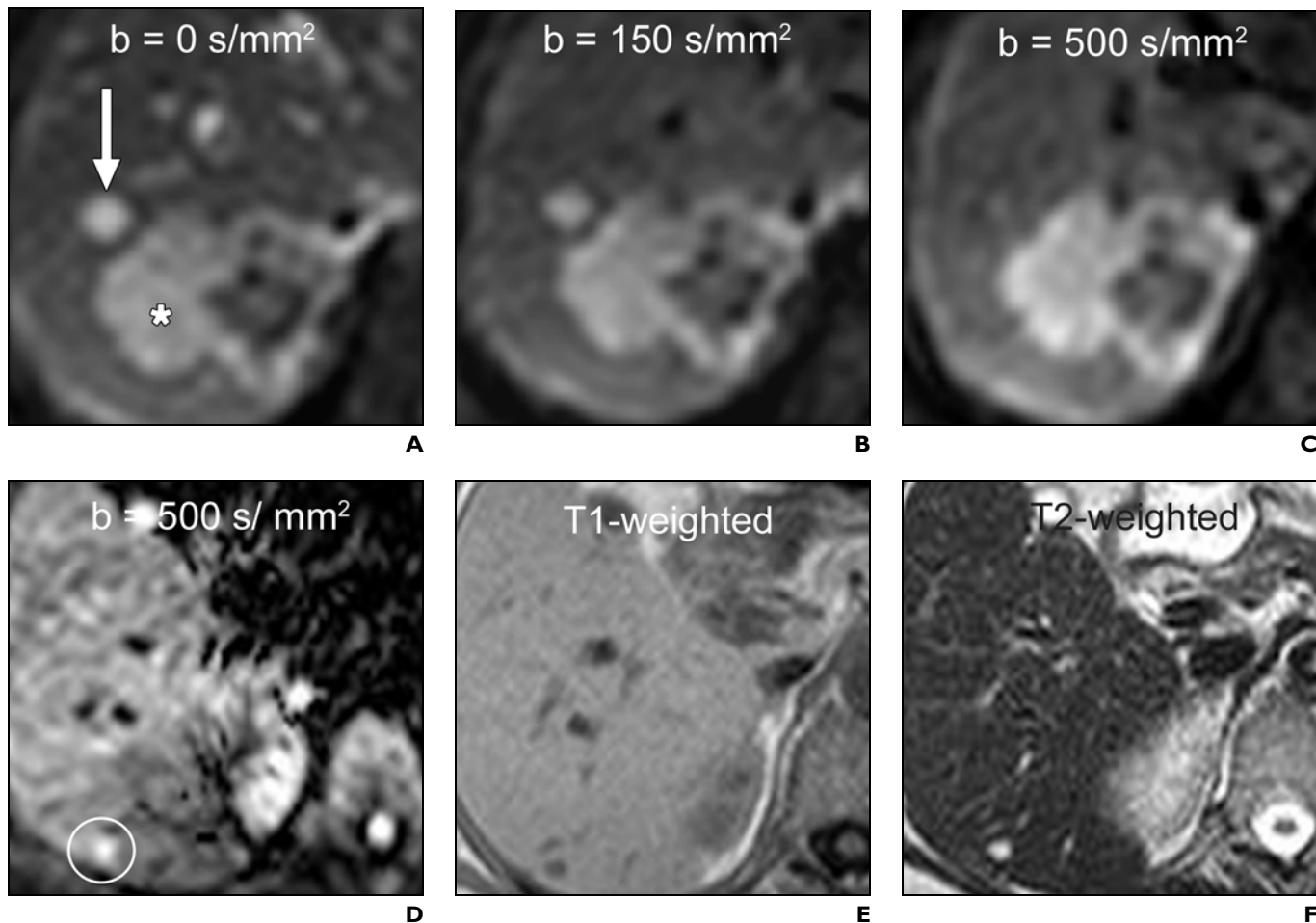


**Fig. 9**—Lesion characterization in 48-year-old man with liver cancer. **A–C**, Diffusion-weighted images show cyst (*arrow, A*) and metastasis (*asterisk, A*) in right lobe of liver. Signal from cyst is attenuated with increasing b value, whereas cellular tumor maintains high signal intensity. **D–F**, Other solid lesions can mimic appearance of metastasis. Hemangioma (*circle, D*) shows restricted diffusion on image obtained with b value of 500 s/mm<sup>2</sup>. However, note typical high T2 signal intensity of lesion. Hence, it is useful to interpret diffusion-weighted imaging sequences with other imaging sequences.

36]. Because of the organization of the renal tubules, water diffusion in the normal kidney is anisotropic [13, 37]. DWI in the kidney can readily distinguish between cystic from solid renal lesions [18]. However, it is not yet possible to confidently distinguish malignant from benign renal neoplasms on the basis of qualitative assessment or ADC measurements [18]. Elsewhere, the ADCs of malignant breast lesions have been found to be lower than the ADCs associated with benign diseases [6, 38, 39], and DWI was able to distinguish cystic soft-tissue sarcomas from solid types [40]. More recently, DWI has also been found to be useful in detecting colorectal carcinoma [41] and showing cystic lesions of the pancreas [42] and ovaries [43].

#### Distinguishing Tumors from Nontumors

In prostate cancer, differentiating tumor from other causes of a low-signal-intensity lesion in the prostate gland is difficult on conventional T2-weighted MRI. Recently, DWI has shown potential for tumor identification [44, 45]. The normal central gland of the prostate has a lower ADC than the peripheral zone [44, 45]. Prostate cancers, which appear as low-signal-intensity foci on ADC maps, typically show lower ADC values than the peripheral zone and the transitional zone and central gland [44, 45]. However, there is significant overlap in the ADC values of prostate cancer and benign prostate changes [44]. Interestingly, investigators have recently observed that low ADC in the central gland and transitional zone accompanied by the loss of glandular anisotropy is more suggestive of tumor than glandular hyperplasia [46].

In the spine, the ability to distinguish a malignant from a nonmalignant cause of vertebral collapse remains challenging. Malignant vertebral infiltration and fracture frequently appear as high-signal-intensity areas on DWI compared with nonmalignant causes [22, 47–51]. A sensitivity of 42–100% and specificity of 92–94% have been reported using visual qualitative assessment [22, 47, 48], although one study found DWI to be unhelpful [52]. By quantitative analysis, malignant vertebral body infiltration and vertebral body fracture return lower ADC values than benign causes [48, 49, 53–56]. A clear separation of ADC measurements between malignant and be-



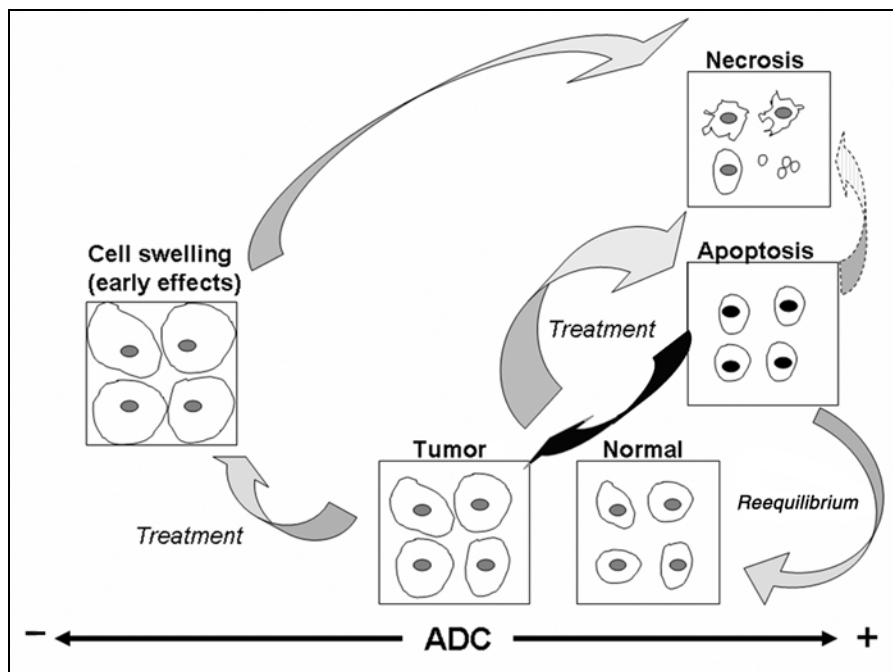


**Fig. 10**—Schematic diagram shows variation in tumor apparent diffusion coefficient (ADC) with treatment. Soon after initiation of chemotherapy or radiation therapy, cell swelling occurs, which can lead to decrease in tumor ADC. This is followed by cell necrosis and lysis, resulting in rise in ADC. Treatment can also induce tumor apoptosis, resulting in cell shrinkage and increased ADC. These apoptotic tumor cells may also undergo secondary lysis (dotted arrow). After completion of treatment, there is process of reequilibrium with resorption of extracellular fluid, leading to decrease in ADC. Tumor regrowth (black curved arrow) can also result in decreased ADC. (Schematic adapted from Moffat et al. [59])

nign groups has been observed [48, 53], but significant overlap has also been reported [56]. Unfortunately, the threshold ADC values that can be applied to discriminate between benign and malignant vertebral disease vary among studies because of differences in the imaging sequences and parameters. Hence, the reader should exercise caution when adopting these criteria for clinical practice. Furthermore, inflammatory conditions, such as tuberculous infection [49] and osteomyelitis [57], can mimic malignant disease on DWI.

One potential use of DWI is in the identification of recurrent or residual tumor after treatment. A recent pilot study in patients with laryngeal cancer showed the potential of the technique to differentiate residual or recurrent tumor from postchemoradiation changes [58]. What was particularly interesting was the fact that DWI could be used to correctly identify a patient as showing posttreatment changes even when PET suggested recurrent disease [58]. Clearly, the promising utility of DWI for this purpose requires further evaluation.

#### Monitoring Treatment Response

There is increasing interest in the application of DWI for detecting tumor response. Effective anticancer treatment results in tumor lysis, loss of cell membrane integrity, increased extracellular space, and, therefore, an increase in water diffusion [59, 60]. The proposed mechanisms in the variation of tumor ADC after the initiation of treatment are summarized in Figure 10 [59].

However, this scheme does not consider the contribution of intravascular perfusion to the diffusion measurement, which may be substantial in a tumor [61]. Hence, therapies that are targeted against tumor vasculature may also result in a reduction in the ADC, especially when the DW images are acquired using low  $b$  values, which are sensitive to vascular perfusion effects [62].

The results of animal studies have confirmed that after the initiation of chemotherapy, radiation therapy, or novel therapy, an increase in the ADC value may be observed in those responding to treatment [62]. Furthermore, treatment effects can be observed within the first 24 hours after initiating treatment [5,

62] due to cell swelling, which results in a transient decrease in the ADC [5, 62].

In human studies of vertebral metastases [50] and brain tumors [63], investigators have reported that treatment response can be observed as a reduction in high signal intensity at DWI. However, such visual appraisal may be confounded by T2 shine-through effects. Using ADC measurements, researchers who have studied hepatocellular carcinoma [64], cerebral gliomas [65], and soft-tissue sarcoma [66] have found that individuals who respond to treatment show a significant rise in the ADC values after therapy. In a recent study of colorectal hepatic metastases, an increase in ADC was observed in patients with at least a partial response to treatment [67]; however, an ADC increase was not observed in the nonresponders [67].

#### Predicting Treatment Response

One of the most intriguing findings associated with the use of DWI in cancer patients has been that ADC measurements appear to be able to predict the response of tumor to chemotherapy and radiation treatment. Table 2 summarizes the findings of selected clinical DWI studies with results that appear to document this phenomenon.

Studies in rectal carcinoma [68, 69], cerebral gliomas [59, 63, 70], and colorectal hepatic metastases [67] have shown that cellular tumor with low baseline pretreatment ADC values respond better to chemotherapy or radiation treatment than tumors that exhibit high pretreatment ADC values. One possible explanation is that tumors with high pretreatment ADC values are likely to be more necrotic than those with low values. Necrotic tumors frequently are hypoxic, acidotic, and poorly perfused, leading to diminished sensitivity to chemotherapy and to radiation therapy.

Studies in cerebral gliomas [59, 63, 71] and breast carcinoma [72] have also shown that an early increase in the ADC after commencing treatment was predictive of better treatment outcome. In two of the studies [71, 72], researchers found that an increase in the ADC within 1 week of initiating treatment was predictive of at least a partial response, with response being defined by tumor size reduction at the end of therapy. The increase in the ADC preceded any reduction in tumor size. The use of ADC to evaluate and predict response has also been assessed in a number of animal studies [62, 73–79] (Table 3).

Many of the clinical studies evaluating DWI for assessing treatment response have been

## DWI Applications and Challenges in Oncology

**TABLE 2: Clinical Diffusion-Weighted Imaging (DWI) Studies Reporting Baseline Apparent Diffusion Coefficient (ADC) Values or Early Changes in ADC Values May Be Used to Predict Response to Treatment**

Authors of Study [reference no.]	Year of Publication	Tumor (no. of subjects)	Treatment	Findings
Moffat et al. [59]	2005	Brain ( <i>n</i> = 20)	Chemoradiation	Increase in ADC at 3 weeks predicted partial response
Theilmann et al. [72]	2004	Metastatic breast ( <i>n</i> = 13)	Chemotherapy	Increase in ADC at days 4–11 predicted treatment response
Mardor et al. [71]	2003	Brain ( <i>n</i> = 10)	Radiotherapy	Increase in ADC at 1 week correlated with subsequent response
Dzik-Jurasz et al. [69]	2002	Rectal cancer ( <i>n</i> = 14)	Chemoradiation	Pretreatment ADC inversely correlated with the percentage tumor reduction
DeVries et al. [68]	2003	Rectal cancer ( <i>n</i> = 34)	Chemoradiation	Tumors with higher percentage of high ADC values responded poorly
Koh et al. [30]	2006	Colorectal liver metastases ( <i>n</i> = 20)	Chemotherapy	High pretreatment ADCs predicted poor response to chemotherapy
Mardor et al. [63]	2004	Brain ( <i>n</i> = 20)	Radiotherapy	Low pretreatment ADC correlated with better response to radiotherapy

**TABLE 3: Assessing Treatment Response of Tumors Using Apparent Diffusion Coefficient (ADC) Measurements in Animal Studies**

Authors of Study [reference no.]	Year of Publication	Journal	Tumor (Animal Model)	Treatment	Findings
Schepkin et al. [78]	2006	<i>Magn Reson Imaging</i>	Subcutaneous gliosarcoma (rats)	1,3-bis(2-chloroethyl)-1-nitrosourea	Increase in ADC after day 2 correlated with response
Thoeny et al. [5]	2005	<i>Radiology</i>	Rhabdomyosarcoma (rats)	Combrestatin A4 phosphate	Decrease in ADC at 1 and 6 h; rise in ADC by day 2 due to tumor necrosis
Jordan et al. [75]	2005	<i>Neoplasia</i>	Human tumor xenografts (rats)	Inhibition of HIF-1 $\alpha$ using PX-478	Decrease of ADC at 24–36 h
Roth et al. [77]	2004	<i>Radiology</i>	C26 colon cancer (mice)	Doxorubicin or aminolevulinic acid-based photodynamic therapy	Low pre-ADC predicted response to chemotherapy; ADC rise at 48 h predicted response to both chemotherapy and photodynamic therapy
Jennings et al. [74]	2002	<i>Neoplasia</i>	Prostate cancer xenografts (rats)	Docetaxel	Significant ADC rise at day 2 after treatment; ADC change correlated with PSA and tumor volume
Stegman et al. [79]	2000	<i>Gene Ther</i>	Orthotopic 9L gliomas	Cytosine deaminase–5-fluorocytosine chemosensitization gene therapy	Increase in ADC indicated drug activity prior to tumor shrinkage
Galons et al. [73]	1999	<i>Neoplasia</i>	Breast tumor xenografts (rats)	Paclitaxel	Early increase in ADC in sensitive tumors but no change in resistant tumors
Lemaire et al. [76]	1999	<i>MAGNA</i>	Mammary tumors (rats)	5-fluorouracil	Tumors with low ADC showed a rise in ADC at day 7

Note—HIF = hypoxia-inducible factor, PSA = prostate-specific antigen.

performed in relatively small numbers of patients. Nevertheless, the body of evidence suggests that ADC measurement is a potentially useful tool that provides unique prognostic information and should be more widely investigated in large clinical studies in the future.

### Whole-Body Imaging

Whole-body DWI is a recently developed application of DWI that, as previously described, is performed using a STIR EPI diffusion-weighted technique with a high *b* value of 1,000 s/mm<sup>2</sup> for background suppression. By performing imaging at multiple stations in the body, a composite image of the whole body can be constructed. The images are processed using maximum inten-

sity projection and are usually displayed using a reversed black-and-white gray scale. Signals from normal tissue such as blood vessels, fat, muscle, and bowel are suppressed. However, other normal structures such as the spleen, prostate, testes, ovaries, endometrium, and spinal cord remain visible [23]. Areas showing restricted diffusion—for example, highly cellular lymph nodes—are strikingly depicted (Fig. 11). Not surprisingly, the technique has been applied to evaluate lymphadenopathy in patients with lymphoma and other cancers. Exquisite images displaying small foci of tumors within the abdomen or peritoneum have also been presented in the literature using this technique [23].

The true utility of whole-body imaging requires further validation. One potential application of DWI is the detection of tumors. This application would be analogous to using whole-body STIR technique for tumor detection. However, because DWI can detect abnormalities on the basis of tissue cellularity, it is unclear whether abnormalities depicted using this technique are necessarily malignant. There is currently a great deal of interest in the development of whole-body DWI with a background-suppression technique. However, more research is needed to establish the sensitivity and specificity of the technique to detect nodal malignancy. Another challenge that must be overcome for DWI to be used for tumor detection is accurate quantification of the ADC.

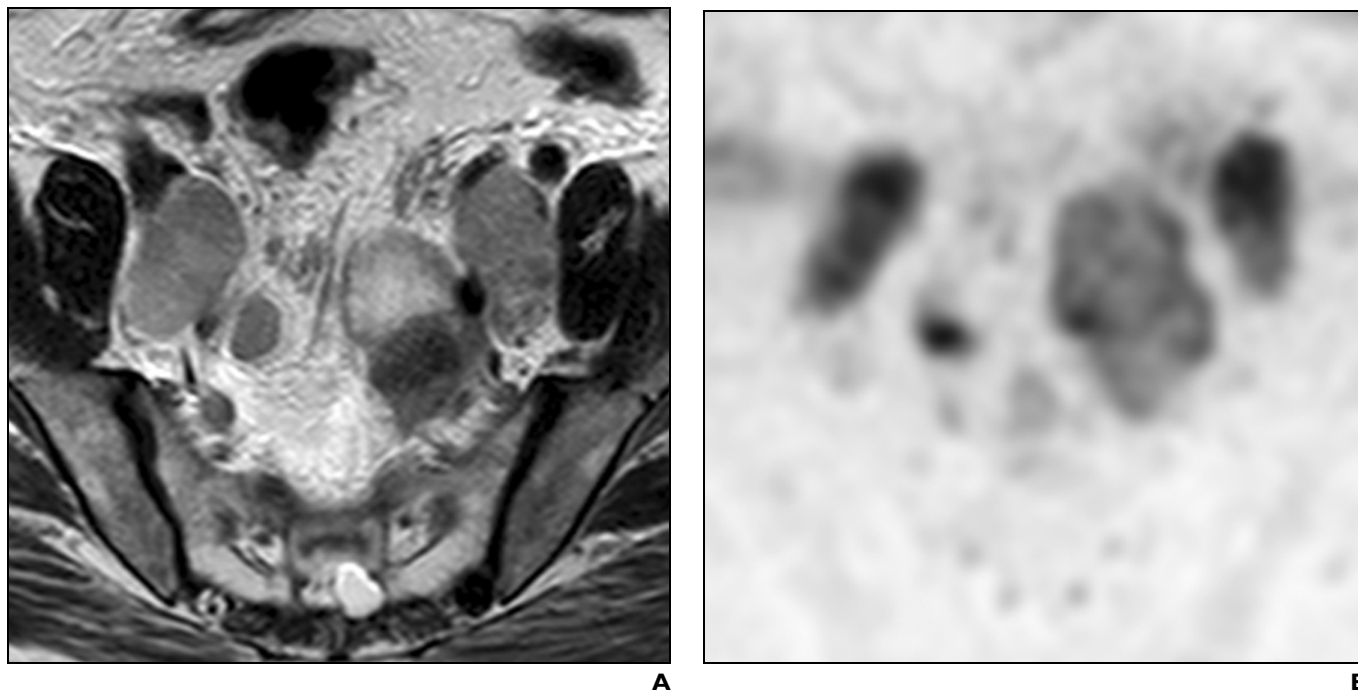


**Fig. 11**—T2-weighted and segment of whole-body diffusion-weighted images.

**A**, T2-weighted image (**A**) and diffusion-weighted inverted gray-scale maximum-intensity-projection ( $b = 1,000 \text{ s/mm}^2$ ) image (**B**) of pelvis show nodal disease along both pelvic sidewalls in 63-year-old man with colon cancer. By performing imaging at multiple stations, whole-body diffusion map can be constructed.

### Current Challenges and Future Developments

One of the greatest challenges to widespread adoption of DWI in the body for tumor assessment is the lack of standardization. The techniques applied to acquire DW images, including the choice of  $b$  values, vary considerably. Consequently, considerable differences in the ADC values of similar diseases have been reported using different techniques. Clearly, future standardization of protocols (e.g., type of sequence, number of motion-probing gradient directions,  $b$  values, and TRs and TEs) for both image acquisition and data analysis across imaging platforms is important.

Current software tools that are available for quantitative analysis on most commercial platforms are fairly basic and do not allow more complex processing. DW images are inherently noisy, and the ability to perform noise filtration may be helpful. Image registration can also help to reduce errors in ADC calculations and further improve the quality of the ADC data. In addition, other metrics, such as fractional anisotropy and perfusion fraction, should be investigated in imaging the patient with cancer. The development and availability of software that allows more sophisticated data analysis would be welcomed.

The tumor microenvironment is both spatially and temporally heterogeneous. By drawing a region of interest around a tumor, the summary statistical value, such as the mean or median value, does not adequately reflect lesion heterogeneity. Clearly, more sophisticated methods of describing the data should be presented, such as the use of histogram analysis or of percentage change in value for 1 pixel [59] between studies.

Despite almost two decades of experience in the use of DWI, little is known about the reproducibility of DWI measurements. Reproducibility measurements are necessary to determine the limits of error in obtaining quantitative ADC measurements to better understand the magnitude of change that can be confidently detected. Reproducibility is particularly important if DWI measurements are to be routinely used for monitoring therapeutic effects in the future.

For clinical drug trials, it is important to understand how the ADC value of a tumor varies temporally with a particular drug treatment. As a tumor responds to treatment, the ADC is likely to rise, but this may undergo reequilibrium after a period of time, leading to a decrease in the ADC. Hence, optimal timing of the measurement is important to maximize the chance of detecting a significant drug effect.

More work is also needed to understand the pathologic changes associated with features observed on DWI. Radiologic–pathologic comparisons are vital in providing robust histologic validation for the observations on DWI.

Although the hardware and software to perform DWI are widely available, the technique has not been routinely applied in clinical practice, especially at extracranial sites. This may in part be due to a lack of recognition by radiologists of DWI as a radiologic tool that provides unique information that can help in tumor evaluation. There is also a lack of instruction available for radiologists who may be interested in adopting the technique for their practice. The availability of training and teaching related to DWI at radiology meetings would help to widen the understanding of the subject and further stimulate interest and research in applications of DWI. Active engagement by radiologists in applying DWI would facilitate its adoption to clinical practice.

### Conclusions

DWI is a powerful imaging tool that provides unique information related to tumor cellularity and the integrity of the cellular membrane. The technique can be applied widely for tumor detection and tumor characteriza-

tion and for the monitoring of response to treatment. In addition, DWI appears to have the ability to predict treatment response to chemotherapy and radiation treatment. Whole-body DWI is a recent development that shows substantial promise for tumor detection, but requires further evaluation. There are, however, major challenges to the widespread adoption of DWI, among which are standardization of data acquisition and analysis. However, because DWI is quick to perform, DWI can be incorporated into standard clinical protocols to be widely evaluated.

References

1. Yoshikawa K, Nakata Y, Yamada K, Nakagawa M. Early pathological changes in the parkinsonian brain demonstrated by diffusion tensor MRI. *J Neurol Neurosurg Psychiatry* 2004; 75:481–484
2. Eastwood JD, Lev MH, Wintermark M, et al. Correlation of early dynamic CT perfusion imaging with whole-brain MR diffusion and perfusion imaging in acute hemispheric stroke. *Am J Neuroradiol* 2003; 24:1869–1875
3. Le Bihan D. Molecular diffusion nuclear magnetic resonance imaging. *Magn Reson Q* 1991; 7:1–30
4. Le Bihan D, Breton E, Lallemand D, Aubin ML, Vignaud J, Laval-Jeantet M. Separation of diffusion and perfusion in intravoxel incoherent motion MR imaging. *Radiology* 1988; 168:497–505
5. Thoeny HC, De Keyzer F, Vandecaveye V, et al. Effect of vascular targeting agent in rat tumor model: dynamic contrast-enhanced versus diffusion-weighted MR imaging. *Radiology* 2005; 237:492–499
6. Guo Y, Cai YQ, Cai ZL, et al. Differentiation of clinically benign and malignant breast lesions using diffusion-weighted imaging. *J Magn Reson Imaging* 2002; 16:172–178
7. Gauvain KM, McKinstry RC, Mukherjee P, et al. Evaluating pediatric brain tumor cellularity with diffusion-tensor imaging. *AJR* 2001; 177:449–454
8. Sugahara T, Korogi Y, Kochi M, et al. Usefulness of diffusion-weighted MRI with echo-planar technique in the evaluation of cellularity in gliomas. *J Magn Reson Imaging* 1999; 9:53–60
9. Lang P, Wendland MF, Saeed M, et al. Osteogenic sarcoma: noninvasive in vivo assessment of tumor necrosis with diffusion-weighted MR imaging. *Radiology* 1998; 206:227–235
10. Stejskal EO, Tanner JE. Spin diffusion measurements: spin-echo in the presence of a time dependent field gradient. *J Chem Phys* 1965; 42:288–292
11. Neil JJ. Measurement of water motion (apparent diffusion) in biological systems. *Concepts Magn Reson* 1997; 9:385–401
12. Inoue T, Ogasawara K, Beppu T, Ogawa A, Kasawara H. Diffusion tensor imaging for preoperative evaluation of tumor grade in gliomas. *Clin Neurol Neurosurg* 2005; 107:174–180
13. Ries M, Jones RA, Basseau F, Moonen CT, Grenier N. Diffusion tensor MRI of the human kidney. *J Magn Reson Imaging* 2001; 14:42–49
14. Taouli B, Martin AJ, Qayyum A, et al. Parallel imaging and diffusion tensor imaging for diffusion-weighted MRI of the liver: preliminary experience in healthy volunteers. *AJR* 2004; 183:677–680
15. Sinha S, Sinha U. In vivo diffusion tensor imaging of the human prostate. *Magn Reson Med* 2004; 52:530–537
16. Bammer R. Basic principles of diffusion-weighted imaging. *Eur J Radiol* 2003; 45:169–184
17. Okada Y, Ohtomo K, Kiryu S, Sasaki Y. Breath-hold T2-weighted MRI of hepatic tumors: value of echo planar imaging with diffusion-sensitizing gradient. *J Comput Assist Tomogr* 1998; 22:364–371
18. Squillaci E, Manenti G, Di Stefano F, Miano R, Strigari L, Simonetti G. Diffusion-weighted MR imaging in the evaluation of renal tumours. *J Exp Clin Cancer Res* 2004; 23:39–45
19. Abe Y, Yamashita Y, Tang Y, Namimoto T, Takahashi M. Calculation of T2 relaxation time from ultrafast single shot sequences for differentiation of liver tumors: comparison of echo-planar, HASTE, and spin-echo sequences. *Radiat Med* 2000; 18:7–14
20. Yamashita Y, Tang Y, Takahashi M. Ultrafast MR imaging of the abdomen: echo planar imaging and diffusion-weighted imaging. *J Magn Reson Imaging* 1998; 8:367–374
21. Ito K, Mitchell DG, Matsunaga N. MR imaging of the liver: techniques and clinical applications. *Eur J Radiol* 1999; 32:2–14
22. Park SW, Lee JH, Ehara S, et al. Single shot fast spin echo diffusion-weighted MR imaging of the spine: is it useful in differentiating malignant metastatic tumor infiltration from benign fracture edema? *Clin Imaging* 2004; 28:102–108
23. Takahara T, Imai Y, Yamashita Y, Yasuda S, Nasu S, Van Cauteren M. Diffusion weighted whole body imaging with background body signal suppression (DWIBS): technical improvement using free breathing, STIR and high resolution 3D display. *Radiat Med* 2004; 22:275–282
24. Moteki T, Sekine T. Echo planar MR imaging of the liver: comparison of images with and without motion probing gradients. *J Magn Reson Imaging* 2004; 19:82–90
25. Nasu K, Kuroki Y, Nawano S, et al. Hepatic metastases: diffusion-weighted sensitivity-encoding versus SPIO-enhanced MR imaging. *Radiology* 2006; 239:122–130
26. Koh DM, Brown G, Riddell A, Scurr E, Collins DJ, Husband JE. Colorectal liver metastases: evaluation using MnDPDP enhanced MR imaging and breath-hold single-shot echo-planar diffusion-weighted MR imaging. *Eur Radiol Suppl* 2005; 15S:B144
27. Brockstedt S, Borg M, Geijer B, et al. Triggering in quantitative diffusion imaging with single-shot EPI. *Acta Radiol* 1999; 40:263–269
28. Murtz P, Flacke S, Traber F, van den Brink JS, Gieseke J, Schild HH. Abdomen: diffusion-weighted MR imaging with pulse-triggered single-shot sequences. *Radiology* 2002; 224:258–264
29. Provenzale JM, Mukundan S, Barboriak DP. Diffusion-weighted and perfusion MR imaging for brain tumor characterization and assessment of treatment response. *Radiology* 2006; 239:632–649
30. Koh DM, Scurr E, Collins DJ, et al. Colorectal hepatic metastases: quantitative measurements using single-shot echo-planar diffusion-weighted MR imaging. *Eur Radiol* 2006; 16:1898–1905
31. Taouli B, Vilgrain V, Dumont E, Daire JL, Fan B, Menu Y. Evaluation of liver diffusion isotropy and characterization of focal hepatic lesions with two single-shot echo-planar MR imaging sequences: prospective study in 66 patients. *Radiology* 2003; 226:71–78
32. Kim T, Murakami T, Takahashi S, Hori M, Tsuda K, Nakamura H. Diffusion-weighted single-shot echoplanar MR imaging for liver disease. *AJR* 1999; 173:393–398
33. Chan JH, Tsui EY, Luk SH, et al. Diffusion-weighted MR imaging of the liver: distinguishing hepatic abscess from cystic or necrotic tumor. *Abdom Imaging* 2001; 26:161–165
34. Koh DM, Scurr E, Collins DJ, et al. Colorectal hepatic metastases: quantitative measurements using single-shot echo-planar diffusion-weighted MR imaging. *Eur Radiol* 2006; 16:1898–1905
35. Yamada I, Aung W, Himeno Y, Nakagawa T, Shibuya H. Diffusion coefficients in abdominal organs and hepatic lesions: evaluation with intravoxel incoherent motion echo-planar MR imaging. *Radiology* 1999; 210:617–623
36. Cova M, Squillaci E, Stacul F, et al. Diffusion-weighted MRI in the evaluation of renal lesions: preliminary results. *Br J Radiol* 2004; 77:851–857
37. Fukuda Y, Ohashi I, Hanafusa K, et al. Anisotropic diffusion in kidney: apparent diffusion coefficient measurements for clinical use. *J Magn Reson Imaging* 2000; 11:156–160
38. Rubesova E, Grell AS, De Maertelaer V, Metens T, Chao SL, Lemort M. Quantitative diffusion imaging in breast cancer: a clinical prospective study. *J Magn Reson Imaging* 2006; 24:319–324
39. Sinha S, Lucas-Quesada FA, Sinha U, DeBruhl N, Bassett LW. In vivo diffusion-weighted MRI of the breast: potential for lesion characterization. *J Magn Reson Imaging* 2002; 15:693–704
40. Dietrich O, Raya JG, Sommer J, Deimling M, Reiser MF, Baur-Melnyk A. A comparative evaluation of a RARE-based single-shot pulse sequence for

- diffusion-weighted MRI of musculoskeletal soft-tissue tumors. *Eur Radiol* 2005; 15:772–783
41. Ichikawa T, Erturk SM, Motosugi U, et al. High-B-value diffusion-weighted MRI in colorectal cancer. *AJR* 2006; 187:181–184
  42. Irie H, Honda H, Kuroiwa T, et al. Measurement of the apparent diffusion coefficient in intraductal mucin-producing tumor of the pancreas by diffusion-weighted echo-planar MR imaging. *Abdom Imaging* 2002; 27:82–87
  43. Moteki T, Ishizaka H. Diffusion-weighted EPI of cystic ovarian lesions: evaluation of cystic contents using apparent diffusion coefficients. *J Magn Reson Imaging* 2000; 12:1014–1019
  44. Issa B. In vivo measurement of the apparent diffusion coefficient in normal and malignant prostatic tissues using echo-planar imaging. *J Magn Reson Imaging* 2002; 16:196–200
  45. Gibbs P, Tozer DJ, Liney GP, Turnbull LW. Comparison of quantitative T2 mapping and diffusion-weighted imaging in the normal and pathologic prostate. *Magn Reson Med* 2001; 46:1054–1058
  46. Junqian G, Humphrey PA, Kibel AS, Narra VR, Song S-K. Exclusion of the false positive identification of prostate cancer using diffusion anisotropy. In: *Proceedings of the International Society of Magnetic Resonance in Medicine meeting*, Seattle, WA. Berkeley, CA: International Society for Magnetic Resonance in Medicine, 2006:174
  47. Baur A, Huber A, Durr HR, et al. Differentiation of benign osteoporotic and neoplastic vertebral compression fractures with a diffusion-weighted, steady-state free precession sequence [in German]. *Rofo* 2002; 174:70–75
  48. Bhugalo AA, Abdullah BJJ, Siow YS, Ng KH. Diffusion-weighted MR imaging in acute vertebral compression fractures: differentiation between malignant and benign causes. *Biomed Imaging Interv J* 2006; 2:e12
  49. Chan JH, Peh WC, Tsui EY, et al. Acute vertebral body compression fractures: discrimination between benign and malignant causes using apparent diffusion coefficients. *Br J Radiol* 2002; 75:207–214
  50. Byun WM, Shin SO, Chang Y, Lee SJ, Finsterbusch J, Frahm J. Diffusion-weighted MR imaging of metastatic disease of the spine: assessment of response to therapy. *Am J Neuroradiol* 2002; 23:906–912
  51. Spuentrup E, Buecker A, Adam G, van Vaals JJ, Guenther RW. Diffusion-weighted MR imaging for differentiation of benign fracture edema and tumor infiltration of the vertebral body. *AJR* 2001; 176:351–358
  52. Castillo M, Arbelaez A, Smith JK, Fisher LL. Diffusion-weighted MR imaging offers no advantage over routine noncontrast MR imaging in the detection of vertebral metastases. *Am J Neuroradiol* 2000; 21:948–953
  53. Herneth AM, Philipp MO, Naude J, et al. Vertebral metastases: assessment with apparent diffusion coefficient. *Radiology* 2002; 225:889–894
  54. Zhou XJ, Leeds NE, McKinnon GC, Kumar AJ. Characterization of benign and metastatic vertebral compression fractures with quantitative diffusion MR imaging. *Am J Neuroradiol* 2002; 23:165–170
  55. Bammer R, Herneth AM, Maier SE, et al. Line scan diffusion imaging of the spine. *Am J Neuroradiol* 2003; 24:5–12
  56. Maeda M, Sakuma H, Maier SE, Takeda K. Quantitative assessment of diffusion abnormalities in benign and malignant vertebral compression fractures by line scan diffusion-weighted imaging. *AJR* 2003; 181:1203–1209
  57. Eastwood JD, Vollmer RT, Provenzale JM. Diffusion-weighted imaging in a patient with vertebral and epidural abscesses. *Am J Neuroradiol* 2002; 23:496–498
  58. Vandecaveye V, de Keyzer F, Vander Poorten V, et al. Evaluation of the larynx for tumour recurrence by diffusion-weighted MRI after radiotherapy: initial experience in four cases. *Br J Radiol* 2006; 79:681–687
  59. Moffat BA, Chenevert TL, Lawrence TS, et al. Functional diffusion map: a noninvasive MRI biomarker for early stratification of clinical brain tumor response. *Proc Natl Acad Sci U S A* 2005; 102:5524–5529
  60. Moffat BA, Hall DE, Stojanovska J, et al. Diffusion imaging for evaluation of tumor therapies in pre-clinical animal models. *MAGMA* 2004; 17:249–259
  61. van Rijswijk CS, Kunz P, Hogendoorn PC, Taminiau AH, Doornbos J, Bloem JL. Diffusion-weighted MRI in the characterization of soft-tissue tumors. *J Magn Reson Imaging* 2002; 15:302–307
  62. Thoeny HC, De Keyzer F, Chen F, et al. Diffusion-weighted MR imaging in monitoring the effect of a vascular targeting agent on rhabdomyosarcoma in rats. *Radiology* 2005; 234:756–764
  63. Mardor Y, Roth Y, Ochershvilli A, et al. Pretreatment prediction of brain tumors' response to radiation therapy using high b-value diffusion-weighted MRI. *Neoplasia* 2004; 6:136–142
  64. Chen CY, Li CW, Kuo YT, et al. Early response of hepatocellular carcinoma to transcatheter arterial chemoembolization: choline levels and MR diffusion constants—initial experience. *Radiology* 2006; 239:448–456
  65. Chenevert TL, McKeever PE, Ross BD. Monitoring early response of experimental brain tumors to therapy using diffusion magnetic resonance imaging. *Clin Cancer Res* 1997; 3:1457–1466
  66. Einarsdottir H, Karlsson M, Wejde J, Bauer HC. Diffusion-weighted MRI of soft tissue tumours. *Eur Radiol* 2004; 14:959–963
  67. Koh DM, Scurr E, Collins DJ, et al. Predicting response of colorectal hepatic metastases: the value of pre-treatment apparent diffusion coefficients. *AJR* (in press)
  68. DeVries AF, Kremser C, Hein PA, et al. Tumor microcirculation and diffusion predict therapy outcome for primary rectal carcinoma. *Int J Radiat Oncol Biol Phys* 2003; 56:958–965
  69. Dzik-Jurasz A, Domenig C, George M, et al. Diffusion MRI for prediction of response of rectal cancer to chemoradiation. *Lancet* 2002; 360:307–308
  70. Oh J, Henry RG, Pirzkall A, et al. Survival analysis in patients with glioblastoma multiforme: predictive value of choline-to-N-acetylaspartate index, apparent diffusion coefficient, and relative cerebral blood volume. *J Magn Reson Imaging* 2004; 19:546–554
  71. Mardor Y, Pfeffer R, Spiegelmann R, et al. Early detection of response to radiation therapy in patients with brain malignancies using conventional and high b-value diffusion-weighted magnetic resonance imaging. *J Clin Oncol* 2003; 21:1094–1100
  72. Theilmann RJ, Borders R, Trouard TP, et al. Changes in water mobility measured by diffusion MRI predict response of metastatic breast cancer to chemotherapy. *Neoplasia* 2004; 6:831–837
  73. Galons JP, Altbach MI, Paine-Murrieta GD, Taylor CW, Gillies RJ. Early increases in breast tumor xenograft water mobility in response to paclitaxel therapy detected by non-invasive diffusion magnetic resonance imaging. *Neoplasia* 1999; 1:113–117
  74. Jennings D, Hatton BN, Guo J, et al. Early response of prostate carcinoma xenografts to docetaxel chemotherapy monitored with diffusion MRI. *Neoplasia* 2002; 4:255–262
  75. Jordan BF, Runquist M, Raghunand N, et al. Dynamic contrast-enhanced and diffusion MRI show rapid and dramatic changes in tumor microenvironment in response to inhibition of HIF-1alpha using PX-478. *Neoplasia* 2005; 7:475–485
  76. Lemaire L, Howe FA, Rodrigues LM, Griffiths JR. Assessment of induced rat mammary tumour response to chemotherapy using the apparent diffusion coefficient of tissue water as determined by diffusion-weighted 1H-NMR spectroscopy in vivo. *MAGMA* 1999; 8:20–26
  77. Roth Y, Tichler T, Kostenich G, et al. High-b-value diffusion-weighted MR imaging for pretreatment prediction and early monitoring of tumor response to therapy in mice. *Radiology* 2004; 232:685–692
  78. Schepkin VD, Chenevert TL, Kuszpit K, et al. Sodium and proton diffusion MRI as biomarkers for early therapeutic response in subcutaneous tumors. *Magn Reson Imaging* 2006; 24:273–278
  79. Stegman LD, Rehemtulla A, Hamstra DA, et al. Diffusion MRI detects early events in the response of a glioma model to the yeast cytosine deaminase gene therapy strategy. *Gene Ther* 2000; 7:1005–1010

Appendix appears on next page

### APPENDIX I: Calculation of Apparent Diffusion Coefficient (ADC)

---

The ADC is calculated mathematically by fitting a decaying exponential function of the form  $S_i = S_0 \times e^{-b \times D}$  to the signal intensity on the  $y$ -axis against the  $b$  values on the  $x$ -axis, where  $S_i$  is the signal intensity of a given pixel;  $S_0$  is the signal intensity of a given pixel without diffusion sensitization;  $e$  is the a mathematical constant, the base of the natural logarithm;  $b$  is the attenuation coefficient ( $\text{mm}^2/\text{s}$ ); and  $D$  is the diffusion rate constant for the given pixel ( $\text{s}/\text{mm}^2$ ).

---